Toward a global magnetospheric equilibrium model

Sorin Zaharia and J. Birn
Space Science and Applications, Los Alamos National Laboratory, Los Alamos, New Mexico, USA

C. Z. Cheng
Princeton Plasma Physics Laboratory, Princeton University, Princeton, New Jersey, USA

Received 25 February 2005; revised 20 June 2005; accepted 24 June 2005; published 29 September 2005.

[1] In this paper we take a first step toward the development of a realistic global magnetospheric model in which the magnetic forces are equilibrated by plasma pressure forces. Such a model describes a ''quasi-static'' equilibrium, a condition valid at most times in the Earth's magnetosphere. The work reported here involves the coupling in two dimensions of a numerical inner/middle magnetosphere model in flux coordinates, which solves the Grad-Shafranov equation in ''inverse'' form, with an asymptotic magnetotail model farther away from Earth. We discuss the obtained configurations (including the resulting magnetic fields and electric currents) under different observation-based inputs (parameters include plasma and total pressures, as well as the magnetic flux boundary). In particular, we focus on the boundary value problem, in which we take realistic shapes for the outer magnetic flux surface (close to the magnetopause) and plasma pressure distributions as model inputs and obtain the total pressure variation in the tail as a by-product of the model.

Citation: Zaharia, S., J. Birn, and C. Z. Cheng (2005), Toward a global magnetospheric equilibrium model, *J. Geophys. Res.*, *110*, A09228, doi:10.1029/2005JA011101.

1. Introduction

[2] Self-consistent (force-balanced) magnetospheric magnetic field models are crucial for many studies in magnetospheric physics, from plasma wave and stability analyses to the study of field-aligned currents. A ''quasi-static'' equilibrium exists in the Earth's magnetosphere during most periods because the flows are sub-Alfvénic [*Wolf*, 1983], except for times of explosive activity such as substorm expansion phases. The evolution of the magnetosphere (including during gradually driven events such as the substorm growth phase) can therefore be portrayed as a time series of such quasi-static equilibria.

[3] Generally a three-dimensional (3-D) magnetic field configuration is not in force balance with any plasma population, and in particular the commonly used existing empirical models are neither likely nor expected to satisfy such balance [*Zaharia and Cheng*, 2003b]. While they are parameterized using many observations, the nonlinearity of the force balance equation together with the variability of magnetospheric states causes deviations from equilibrium in such models. Therefore, for applications in which force balance is required, equilibrium configurations have to be explicitly computed.

[4] Two major approaches have been developed in the area of 3-D numerical magnetospheric equilibrium modeling: a ''magnetofrictional'' MHD approach [*Hesse and Birn*, 1993; *Lee et al.*, 1995; *Toffoletto et al.*, 2001; *Lemon et al.*, 2003] and an iterative solution with prescribed pressure in flux coordinates (Euler potentials) [*Cheng*, 1995; *Zaharia et al.*, 2004] (for a comprehensive review of various numerical methods for solving the plasma equilibrium, see *Takeda and Tokuda* [1991]). The magnetofrictional approach essentially consists of solving the fully dynamic MHD equations, albeit with an artificial damping term, to approach a final equilibrium, which is given by the fields as functions of the three space coordinates. In contrast, the Euler potential approach, to be described in more detail in section 2.1, permits a reduction of the problem to an iterative solution of ''quasi 2-D'' equations, with the final equilibrium obtained in ''inverse'' form, that is, the Cartesian coordinates of the points defining field lines given as functions of the flux coordinates.

[5] Between the two methods mentioned above, currently only the latter one in flux coordinates is generalized to include anisotropic pressure (for a more detailed discussion of differences between the two methods, the reader is directed to *Zaharia et al.* [2004, section 2.3]). Computations have been performed using this approach with pressure and anisotropy degree from observations or kinetic models [*Zaharia and Cheng*, 2003a; *Zaharia*, 2003; *Zaharia et al.*, 2004, 2005], leading to both quiet and active time force-balanced magnetospheric states.

[6] Still, the computational flux coordinate approach discussed above has numerical limitations that prevent its use past 25 R_E in the magnetotail, because of the need of maintaining ''nested'' magnetic flux surfaces. Beyond about 20 R_E in the tail however, an approximate calculation can be used, the so-called ''tail approximation'' of *Birn*

0148-0227/05/2005JA011101$09.00

[1987]. That approach, also employing the Euler potential representation, assumes that the total pressure is independent of the GSM Z coordinate, an assumption that becomes valid at around 20 R_E from Earth. The tail approximation greatly simplifies the 3-D equilibrium problem by reducing it to the integration of simple ordinary differential equations.

[7] This article presents the coupling between the two approaches mentioned (the inner and the tail models) in the simpler 2-D case, performed through a "line-tying" technique, facilitated by the similar Euler potential representation in both models. The 2-D line-tying approach will in the future be applied to the full 3-D problem, which in the interior region is a set of "quasi 2-D" equations in flux coordinates [*Zaharia*, 2003].

[8] The paper is organized as follows: in section 2 we summarize the theory of the two models to be coupled, first in full 3-D geometry, as well as the particularization to two dimensions. Section 3 presents numerical details of the iterative coupling procedure through a planar interface in the magnetotail, including a technique for ensuring that the numerical mesh is non-self-overlapping. Section 4 describes configurations obtained using the coupled model with different choices of plasma/total pressure, as well as outer flux boundary shape. The focus is on the boundary value problem, treated before in the tail [*Birn*, 1991]. In this problem we specify (from an empirical model) the shape of the outer magnetic flux surface (close to the magnetopause) and the plasma pressure (observation-based), obtaining as a by-product the total pressure variation in the tail. Then, section 5 presents additional discussion of the results and compares them with previous results/observations. Finally, section 6 summarizes the paper and sets forth several conclusions.

2. Theory of the Constituent Models

[9] Both models tackle the standard equations describing magnetostatic equilibrium, which for the particular case of isotropic pressure have the form

$$\mathbf{j} \times \mathbf{B} = \nabla P \tag{1}$$

$$\nabla \times \mathbf{B} = \mu_0 \mathbf{j} \tag{2}$$

$$\nabla \cdot \mathbf{B} = 0. \tag{3}$$

[10] The model coupling is greatly facilitated by the fact that the magnetic field is expressed in both models in terms of Euler potentials [*Stern*, 1970]:

$$\mathbf{B} = \nabla\alpha \times \nabla\beta. \tag{4}$$

Equation (4) shows that the intersection of constant α and β surfaces defines the magnetic field lines.

2.1. Inner/Middle Magnetosphere 3-D Equilibrium

[11] With the magnetic field expressed by equation (4), one can construct a flux coordinate system $\{\alpha, \beta, \chi\}$ (a note of caution: for clarity purposes we use the same notation here, α and β, for the pair of Euler potentials defining the field in both the inner and the tail model; this notation is the same as the one used by *Birn* [1987] and is common in the space physics community; it is however a change from the (ψ, α) terminology commonly used in fusion plasmas and employed in our previous flux coordinate equilibrium work).

[12] For the magnetospheric case, α can be chosen to be a magnetic flux function, and then the other potential (β) is a periodic azimuthal angle-like function, not equal to the longitudinal angle in general. The third function χ completing the flux coordinate system is a generalized "poloidal" angle, and is a function of the distance along the field line. Very near the Earth (within 2 R_E) a constant α surface can be well approximated by an L shell of the dipole field, while β there is very close to the longitudinal angle. The flux coordinate system is generally not orthogonal, with $\nabla\alpha \cdot \nabla\beta \neq 0$, $\nabla\alpha \cdot \nabla\chi \neq 0$ and $\nabla\beta \cdot \nabla\chi \neq 0$.

[13] The equilibrium method in flux coordinates allows one to specify an arbitrary pressure tensor [*Zaharia*, 2003]. For the case of isotropic pressure, because $\mathbf{B} \cdot \nabla P = 0$, the pressure is constant along the field line: $P = P(\alpha, \beta)$. Decomposing the force balance equation (1) along the directions $\mathbf{B} \times \nabla\alpha$ and $\mathbf{B} \times \nabla\beta$, respectively, one obtains

$$\mathbf{j} \cdot \nabla\alpha = \frac{1}{\mu_0} \nabla \cdot \left[(\nabla\alpha)^2 \nabla\beta - (\nabla\beta \cdot \nabla\alpha) \nabla\alpha \right] = -\frac{\partial P}{\partial \beta} \tag{5}$$

$$\mathbf{j} \cdot \nabla\beta = \frac{1}{\mu_0} \nabla \cdot \left[(\nabla\beta \cdot \nabla\alpha) \nabla\beta - (\nabla\beta)^2 \nabla\alpha \right] = \frac{\partial P}{\partial \alpha}. \tag{6}$$

Equations (5) and (6) are elliptic equations for β and α on each constant α and β surface, respectively. In the axisymmetric limit, equation (5) is trivially satisfied by $\beta \equiv \phi$. Equation (6) is a generalized Grad-Shafranov equation. In general (5) and (6) are three-dimensional equations. However, in the $\{\alpha, \beta, \chi\}$ system we can reduce their dimensionality to 2-D. They are a coupled set of "quasi 2-D" equations that can be solved by specifying boundary conditions for α and β as well as the $P(\alpha, \beta)$ distribution at an arbitrary location on each field line.

[14] A numerical 3-D code has been developed to solve the nonlinear equilibrium equations above [*Cheng*, 1995; *Zaharia*, 2003; *Zaharia et al.*, 2004]. The numerical grid is tied to the equilibrium solution in such a way that grid points automatically accumulate in regions of steep gradients, thus yielding accurate solutions of high plasma beta (β_p) equilibria. An iterative metric method [*DeLucia et al.*, 1980] is used to solve for the discrete Cartesian coordinates $X(\alpha, \beta, \chi)$, $Y(\alpha, \beta, \chi)$ and $Z(\alpha, \beta, \chi)$ defining constant α and β surfaces such that the finite differenced equations based on these points are satisfied to a small tolerance. The fixed-boundary problem is solved inside a domain bounded by (1) an outer $\alpha = \alpha_{out}$ flux boundary, with shape specified to take into account the effects of the solar wind and interplanetary magnetic field (IMF); (2) an inner $\alpha = \alpha_{in}$ boundary primarily determined by the Earth's magnetic field; and (3) the Earth's surface (or a sphere of radius r enveloping the Earth) between the α_{in} and α_{out} surfaces. The boundary condition for β on the inner sphere is $\beta = \phi$. The flux boundaries, $\alpha = \alpha_{out}$ and $\alpha = \alpha_{in}$ delimiting the

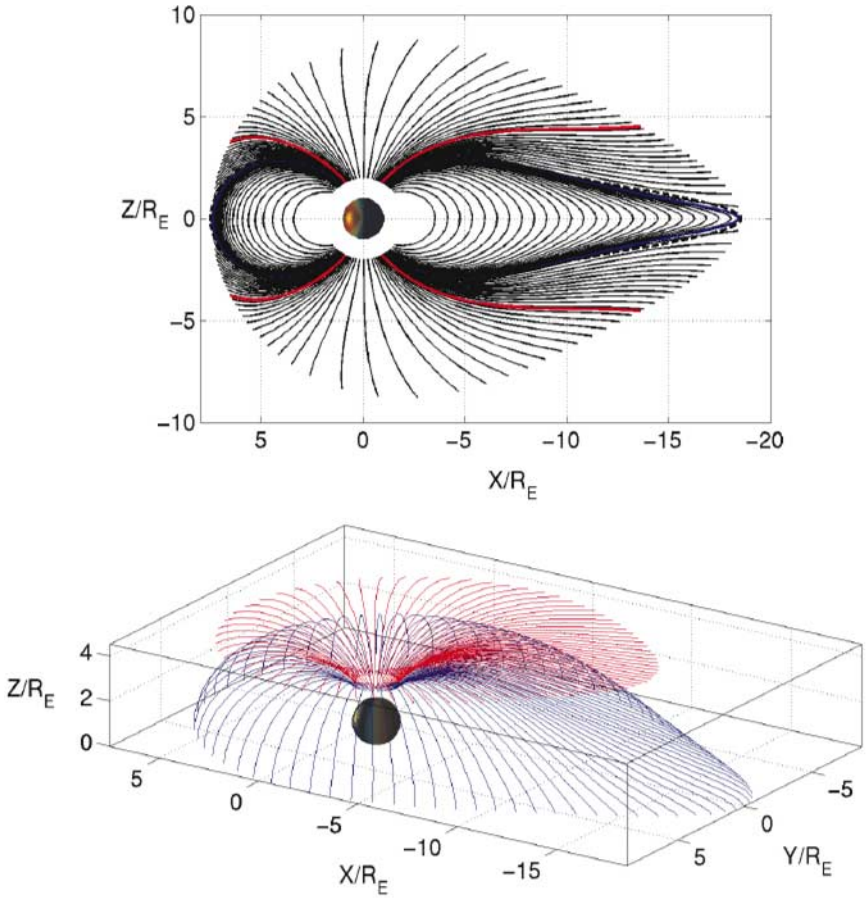

Figure 1. (top) Noon-midnight meridian picture of constant magnetic flux (α) surfaces for a computed 3-D equilibrium with "open field" regions included. The thick black dashed line is the outer closed α surface at the beginning of the computation, that is, obtained from the empirical model. (bottom) Three-dimensional view of field lines with two different α in the Northern Hemisphere: the last "closed field" α (blue) and an open field α (red). The lines with the same α are shown in the same colors in the top plot as well [from *Zaharia*, 2003].

domain have shapes usually obtained by field line tracing using empirical models such as T96 [*Tsyganenko and Stern*, 1996] or T01 [*Tsyganenko*, 2002], with various solar wind and IMF conditions.

[15] Besides boundary conditions, the method requires specifying the P distribution at one location on each field line for a unique solution. It is usually given in the equatorial plane from either direct observations [*Lui and Hamilton*, 1992; *De Michelis et al.*, 1999], or indirectly through empirical formulas [*Spence and Kivelson*, 1993].

[16] The numerical code was used to obtain 3-D quasi-static equilibria in the closed field region under different solar wind conditions and with both isotropic and anisotropic pressure [*Zaharia and Cheng*, 2003a; *Zaharia et al.*, 2004]. We have also recently extended [*Zaharia*, 2003] the computational domain from the closed field region to cover high-latitude, sometimes open field lines as well. The domain was again constructed by field line tracing using empirical models. It was limited in the "open field" regions by cutting the lines as they touched an "eggshell" surface (Figure 1) obtained by the rotation of an equatorial closed contour around the x axis. Inside the whole volume delimited by that surface equations (5) and (6) were solved iteratively, using a modified Spence-Kivelson pressure profile [*Spence and Kivelson*, 1993] in the equatorial plane and an analytical extension of $P(\alpha, \beta)$ in the "open" region (for computation purposes, whether the "open" field lines that are cut at the boundary are indeed open to the IMF or close farther in the tail is not relevant). Continuity of physical quantities at the open-closed boundary was maintained throughout the iterations. Having in place the methodology to treat both closed and open field regions in the interior equilibrium code allows a coupling with the tail equilibrium model that will cover all α values (all latitudes).

2.2. Magnetotail Model

[17] We now briefly describe the "tail equilibrium" model [*Birn*, 1987]. The magnetic field in this approach is also expressed in terms of Euler potentials by equation (4) (in general α and β here need not be the same as the ones in section 2.1). The model relies on the fact that under typical magnetotail conditions, excluding the inner magnetosphere and the magnetopause boundary regions, the characteristic scale length L_Z for variations in Z, equivalent to the

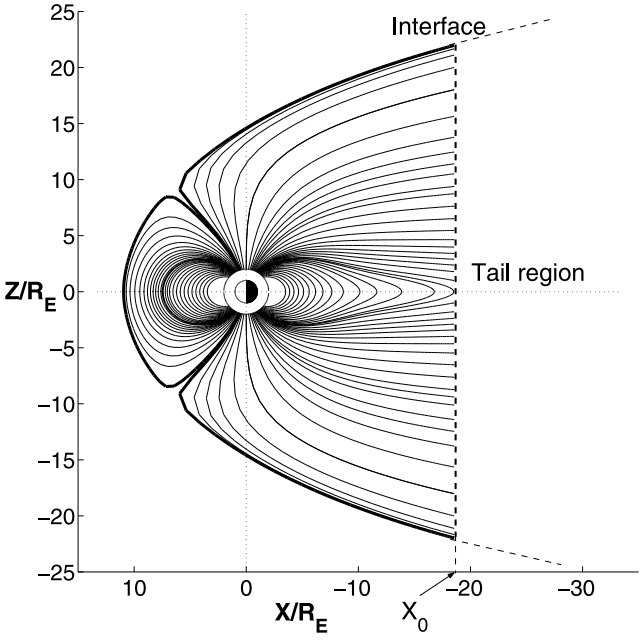

Figure 2. Picture in the noon-midnight meridian of a domain bounded by a (closed) magnetopause (thick solid lines), defined by the T96 model (with northward IMF); inside the domain, a numerical equilibrium is sought. Interior field lines are also obtained by field line tracing using T96, to be employed as an initial "guess" for the inner computation. The domain is limited in the tail by a plane perpendicular to the x axis, at a distance X_0 where the "tail approximation" starts to become valid; approximate tail solutions are sought beyond X_0.

characteristic current or plasma sheet half thickness, is of the order of a few R_E or smaller, whereas the variations along X and Y occur on scales of the order of 10 to tens of R_E. In other words, the "tail approximation" is the ordering

$$B_Z, \partial/\partial X, \partial/\partial Y = \mathcal{O}(\epsilon),\ \epsilon^2 \ll 1.$$

[18] Under these conditions, the curvature term in the Z component of equation (1) is small and the pressure balance becomes [e.g., *Siscoe*, 1972]

$$P + \frac{B^2}{2\mu_0} = \hat{P}(X, Y), \tag{7}$$

where $\hat{P}$ is the total pressure. As shown by *Birn* [1987], equations (1) and (2) can then be reduced to a set of ordinary differential equations for the case of isotropic pressure:

$$\begin{aligned} dX/d\tau &= B_X \\ dY/d\tau &= B_Y \\ dB_X/d\tau &= \mu_0 \partial\hat{P}/\partial X \\ dB_Y/d\tau &= \mu_0 \partial\hat{P}/\partial Y \end{aligned} \tag{8}$$

and an integral

$$Z = \int |\nabla\beta|_\alpha \frac{d\alpha}{\sqrt{2\mu_0[\hat{P} - P(\alpha,\beta)]}} + Z_0(X, Y). \tag{9}$$

Here τ is a variable

$$\tau = \int \frac{ds}{B} \tag{10}$$

expressing the differential flux tube volume integrated along a field line, such that $d/d\tau \equiv \mathbf{B}\cdot\boldsymbol{\nabla}$ represents the derivative along a field line, that is, for constant α and β.

[19] Equation (8) yields the field line projections in the (X, Y) plane, $X = X(\alpha, \beta, \tau)$, $Y = Y(\alpha, \beta, \tau)$, while equation (9) gives the Z coordinate of the field lines as a function of X and Y, using the solution of equation (8) to express β as a function of X, Y, and α. The gradient of β in equation (9) is to be understood as the gradient for constant α. The potentials α and β enter the solutions via the boundary conditions. The function $Z_0(X, Y)$ can be chosen as the location of the neutral sheet. The tail equilibrium solutions, like the inner numerical ones, are therefore achieved as explicit representations of the field lines.

[20] The solutions of equations (8) and (9) are governed by two functions, the total pressure $\hat{P}(X, Y)$ and the plasma pressure function $P(\alpha, \beta)$. In the coupling of the two models, $P(\alpha, \beta)$ will be taken at the coupling interface from the calculation in the inner region. The total pressure function $\hat{P}(X, Y)$ then determines how the configuration continues into the tail under equilibrium conditions. It can be taken from various sources: empirical models, observations, global simulations or it can be designed from first principles. For example, from equation (7) $\hat{P}$ is approximately equal to the magnetic pressure in the lobes, where plasma pressure is negligible. Therefore lobe measurements [e.g., *Slavin et al.*, 1985; *Fairfield and Jones*, 1996] could be one source for specifying $\hat{P}$. An alternative to taking $\hat{P}$ as an input is the boundary value problem [cf. *Birn*, 1991], in which one specifies the shape of the outer magnetic flux surface (for example from empirical models) and either the plasma pressure or the total pressure function.

3. Model Coupling: 2-D Solution

3.1. General Coupling Issues

[21] The fact that both models describe the magnetic configuration as an explicit field line representation (i.e., X, Y and Z as functions of α, β and χ) allows for a coupling through a "line-tying" approach, performed at a planar interface at distance X_0 where the tail approximation becomes valid (see Figure 2). The domain in Figure 2, with the outer flux surface α_{out} being the magnetopause, is obtained by tracing of an empirical model field and cutting of the traced field lines as they touch a plane perpendicular to the x axis at $X = X_0$. In our work here we will not take the outer flux surface to be the magnetopause, but rather the field line (close to the magnetopause) starting from the pole on the Earth's surface.

[22] As discussed, the tail model will be run with either total pressure or boundary shape inputs. If the total

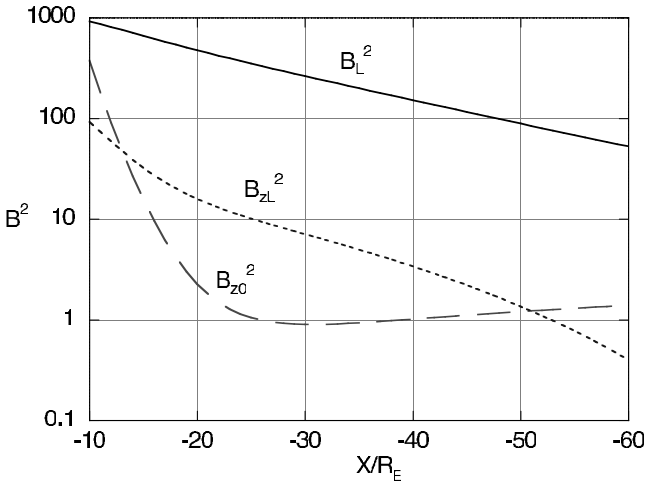

Figure 3. Variation of magnetic pressure contributions in the T87 model (for $Kp = 0$ and zero tilt) along the tail at $Y = 0$. B_L (solid line) is the total lobe field (evaluated at $Z = 15$ R_E), B_{ZL} (dotted line) is its Z component, and B_{Z0} (dashed line) is the equatorial B_Z. The figure shows that the pressure contributions from B_Z are a few percent of the lobe field contribution tailward of $X \simeq -15$ R_E.

pressure is specified, the relationship between plasma pressure and the lower bound $\hat{P}_{\min}$ of $\hat{P}(X, Y)$ directly determines which lines are open, since only field lines with a pressure above $\hat{P}_{\min}$ can cross the neutral sheet [*Wiechen and Schindler*, 1988; *Birn et al.*, 1992]. Therefore the equilibrium tail structure follows largely from the total pressure function, and major mapping features, such as the location of the distant neutral line, can be derived (or imposed by the choice of $\hat{P}(X,Y)$) even without having to integrate field lines. With the boundary specified, the same characteristics are determined by the interplay between plasma pressure and the boundary shape.

[23] The tail model provides the foot points of the field lines on the coupling interface, which are used as boundary conditions for the "open" field lines in the inner model. Conversely, the inner model provides the pressure on each field line connected to the tail. An iterative approach is employed back and forth between the two models until convergence to a final equilibrium solution.

[24] On the basis of the empirical T87 model [*Tsyganenko*, 1987], Figure 3 suggests that a tail distance between 15 and 20 R_E is suitable for the coupling interface, because B_Z^2 becomes reduced there to only a few percent of the lobe magnetic pressure, equivalent to the total pressure.

3.2. Two-Dimensional Case

[25] Because the inner 3-D solution consists in successive solutions of "Grad-Shafranov-like" 2-D equations for one Euler potential on surfaces on which the other is constant, a line-tying approach will provide boundary conditions for a 2-D equation at a time. It is useful therefore to solve the less complex problem of 2-D equilibrium before tackling the full 3-D solution. The 2-D coupling will be the focus of this paper from here on, while also considering a zero Earth dipole tilt (north-south symmetry); the extension to a tilted dipole is straightforward.

[26] In the 2-D case (with $B_Y = 0$) in the midnight meridian, while taking the field invariant in Y in the tail, we consider it axisymmetric in the inner region (the **B** field cannot be invariant in Y near Earth as that would require a line dipole instead of the Earth dipole). Introducing the two-dimensional flux function A, the field representation in the two regions and the coupling condition are

$$\mathbf{B}_{\text{inner}} = \nabla\alpha \times \nabla\phi \tag{11}$$

$$\mathbf{B}_{\text{tail}} = \nabla A \times \nabla Y \tag{12}$$

$$\alpha|_{X=X_0} = -X_0 A|_{X=X_0}, \tag{13}$$

where $X_0 < 0$ is the location of the coupling interface in the tail.

[27] The 2-D equilibrium is described by the Grad-Shafranov equation for α in the inner region (equation (6) with $\beta \equiv \phi$), while in the tail solution (9) becomes

$$Z(X,A) = \int_{A_0}^{A} \frac{dA'}{\sqrt{2\mu_0\left[\hat{P} - P(A')\right]}} + Z_0(X), \tag{14}$$

where $Z_0(X)$ is the Z location of the field line $A = A_0$.

3.3. Numerical Issues

[28] The interior model requires specifying a starting configuration as an "initial guess" in the iterative computation. In our previous equilibrium work, we took such a guess from the empirical models that also provided the boundaries. An issue arises in the coupling however because as the tail model provides new foot points for the field lines at the boundary, the interior computational points have to be redistributed; that is, a new "guess" configuration must be found for the next iteration. If the Z values provided by the tail model are very different from the boundary foot points at the previous step, just changing the locations of the end points on the field lines could lead to lines touching one another (also known as mesh "self-overlapping"), thus violating the nested-flux assumption critical for the interior numerical solution.

[29] A method is therefore needed to smooth the mesh. For this, we perform a "boundary-conforming" mapping [e.g., *Wang and Tang*, 2005]. We first take as an initial guess for each field line a fourth-order Bezier curve with anchor points fixed on the Earth's surface and at the matching boundary. The tangents of the field lines are set to match the dipole and tail field tangents, respectively. Initially, the fifth control point of each curve is left arbitrary. In general, such a set of Bezier curves does not guarantee a nonself-overlapping mesh. We can however obtain a good mesh by imposing a specific condition as a criterion for finding the coordinates of the fifth control point. Following

the method described by *Wang and Tang* [2005], we construct a functional

$$\Pi = \sum_{k\in I}\left[\frac{\partial X}{\partial t}\frac{\partial X}{\partial \rho}+\frac{\partial Z}{\partial t}\frac{\partial Z}{\partial \rho}\right]_k^2 + \lambda\sum_{k\in I}\left\{\max\left[\frac{\partial \mathrm{X}}{\partial \rho}\frac{\partial \mathrm{Z}}{\partial \mathrm{t}}-\frac{\partial \mathrm{X}}{\partial \mathrm{t}}\frac{\partial \mathrm{Z}}{\partial \rho}\right]_{\mathrm{k}},0\right\}^2 \quad (15)$$

with the sums performed over all points k in the mesh I. The variables $t \in [0, 1]$ and $\rho \in [0, 1]$ are computational flux coordinates, such that at equilibrium $t = t(\chi)$ and $\rho = \rho(\alpha)$. The first term in equation (15) is related to mesh orthogonality, while the second (related to the Jacobian of the transformation from Cartesian coordinates to flux coordinates) describes self-overlapping (a positive Jacobian everywhere ensures a non-overlapping mesh). We then use a conjugate gradient method [*Press et al.*, 1992] to find the coordinates that lead to a minimum in Π and thus ensure a well-behaved (non self-overlapping) mesh. The parameter λ is varied during the calculation, from a smaller value initially to a larger one later.

[30] After the mesh is built, we apply a Picard iteration technique to find the interior solution, such that at step $n + 1$ we use the right-hand side computed from the quantities at step n. The Grad-Shafranov equation is solved at each step via SOR iteration with Chebyshev acceleration [*Press et al.*, 1992] (a direct block tridiagonal method is also implemented). The iterative process is performed until convergence, defined [*Zaharia et al.*, 2004] as the moment when the relative force imbalance $f_n = \|F_n\|/\|F_0\|$ decreases by about 2 orders of magnitude. Here F_0 and F_n are the force balance imbalance before the computation and at step n, respectively, defined as

$$\|F\| = \frac{\int |\mathbf{j}\times\mathbf{B}-\nabla P|dV}{\int dV}. \quad (16)$$

[31] In order to improve numerical convergence for the interior computation we also use an "under-relaxation" or "blending" technique [*Mouschovias*, 1974; *Zaharia et al.*, 2004], whereby some fraction of the solution of the previous iteration is "blended" into the latest solution: $\alpha^{(n+1)} \leftarrow \gamma_\alpha\alpha^{(n)} + (1 - \gamma_\alpha)\alpha^{(n+1)}$, where γ_α is the blending parameter. Obviously, the larger the "blending parameter" γ, the less change between two consecutive iterations, and the more iterations are needed for convergence.

[32] In the work presented here we use 75×75 computational grid points, and typically 30 iterations are necessary for the coupled code to converge. We have also performed computations with more (101×101) and less (51×51) and obtained very similar final configurations.

4. Results for 2-D Coupling

4.1. Prescribing $P(\alpha)$ and $\hat{P}(X)$

[33] In this coupling scheme, we prescribe in the tail model the plasma pressure $P(\alpha)$ (from the inner region) as well as the total pressure function $\hat{P}(X)$. The shape of the outer flux boundary $a(X)$ is then obtained as a solution to the problem. We present here a quiet-time configuration obtained through this approach. In the inner closed region (for field lines that close through the equatorial plane closer to Earth than the matching boundary), we do not use a specified function $P(\alpha)$, but rather an observation-based dependence of P on X, the so-called Spence-Kivelson profile [*Spence and Kivelson*, 1993]:

$$P(X)|_{Z=0}(\mathrm{nPa}) = 89\mathrm{e}^{-0.59|\mathrm{X}|} + 8.9|\mathrm{X}|^{-1.53}. \quad (17)$$

[34] This profile has been shown [*Zaharia and Cheng*, 2003b] to approximately equilibrate a quiet-time T96 magnetic field on the noon-midnight meridian line. The functional $P(\alpha)$ in the closed field region then changes at each iteration until equilibrium. In the "open field" region, since we do not have an observation-based spatial dependence available, we use an analytic extension:

$$P_{\mathrm{open}}(\alpha) = P_0 + (P_N - P_0)\exp\left\{-C\frac{\alpha-\alpha_n}{\alpha_n-\alpha_1}\right\}, \quad (18)$$

where α_1 and α_n are the flux values for the first and last "closed" flux surfaces, respectively. The constants P_N and P_0 are found from the pressure continuity at the open-closed boundary, as well as from the value of the plasma pressure in the lobes (on the field line with $\alpha = 0$). The choice of an exponential added to P_0 in equation (18) is inspired by the Harris current sheet [*Harris*, 1962] and by typical tail models [e.g., *Birn*, 1987]. The lobe pressure (very close to P_0) can be reasonably taken to be on the order of 10^{-2} nPa during quiet times, as most in situ observations suggest (e.g., *Tsyganenko* [2000], using ISEE 2 observations, finds at 20 R_E a typical lobe plasma β_p of 4% and a typical plasma pressure of 0.01 nPa). The remaining parameter C is found at each iteration from the continuity of $dP/d\alpha$ at the open-closed field boundary.

[35] For the total pressure variation in the magnetotail we use a power law dependence of a form similar to that used by *Birn* [1987]:

$$\hat{P}(X) = \hat{P}_0\left(\frac{X_0}{X}\right)^m. \quad (19)$$

[36] In the inner region only, we need a flux boundary choice, and we take it from the T96 empirical model [*Tsyganenko and Stern*, 1996], with parameters representing average quiet-time conditions [*Zaharia et al.*, 2004]: $B_{\mathrm{ZIMF}} = 1$ nT, $B_{\mathrm{YIMF}} = 0$, $Dst = -5$ nT and $P_{\mathrm{SW}} = 2.1$ nPa. Since in this case the total pressure is given at the matching boundary from the inner region, we also need a lobe plasma pressure value ($\simeq P_0$) such that the "magnetopause" location there coincides with that (from T96) in the inner region. We find that $P_0 = 0.031$ nPa gives the best match for a quiet-time case (alternatively, $\hat{P}$ can be found at the matching boundary by taking $a[\hat{P}(X_0)]$ there and inverting it).

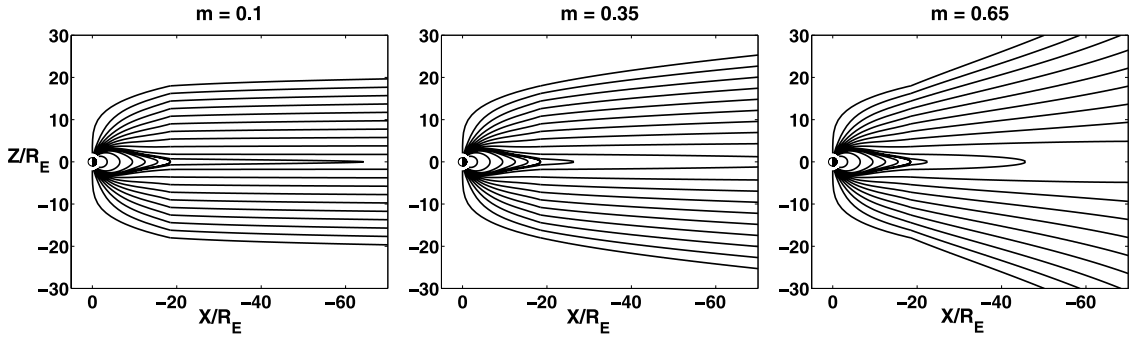

Figure 4. Equilibrium field line geometry for three different choices for m in the variation of $\hat{P}(X)$ (equation (19)).

[37] The form of the pressure function (18) allows for an analytical solution for the field lines, in the form (in the normalized units in the code)

$$Z(\hat{P},\alpha) = \frac{\sqrt{2}(\alpha_n - \alpha_1)}{C|X_0|\sqrt{\hat{P} - P_0}} \operatorname{atanh}\sqrt{\frac{\hat{P} - P(\alpha)}{\hat{P} - P_0}}. \qquad (20)$$

[38] This can also be interpreted as a solution $Z(X, \alpha)$, since we know $\hat{P}(X)$. Replacing $\alpha = 0$ in equation (20) gives the shape of the outermost magnetic field line, $a(X)$.

[39] Figure 4 shows the field line geometry in the final equilibrium configurations for three different choices of the $\hat{P}$ variation: $m = 0.1$, 0.35 and 0.65. It is clear that too small m (very slow decrease of $\hat{P}$) leads to a flat outer flux surface, in disagreement with observations [e.g., *Shue et al.* 1997] showing an increase in the tail radius with distance. The choice $m = 0.1$ also leads to a field curvature in the tail much larger than in the inner region, that is, a jump in the field value at the matching boundary. On the other hand, too large m (rapid decrease of $\hat{P}$) causes an unrealistically large magnetotail flaring, much larger than observed. Therefore magnetopause shape observations are an additional constraint on model parameters, with only a restrictive range allowed for the total pressure variation.

[40] The optimal m ($m = 0.35$) would correspond (since $\hat{P} \propto B^2_{\rm lobe}$) to a tail lobe field variation with distance with a power of 0.175. This is much lower than observed [*Fairfield and Jones*, 1996] and is likely an effect of the two-dimensional approximation. In the full 3-D case, for a given variation of lobe field with distance, the existence of the additional tail flaring in the Y direction will decrease the flaring in Z [*Birn et al.*, 2004], allowing the larger observed variation of the lobe field (or total pressure) while keeping the flaring in Z realistic. Therefore, rather than claiming that $m = 0.35$ is a realistic value for the $\hat{P}$ behavior in reality, we only stress that observations do impose a constraint on the total pressure variation. We also note that in this coupling approach, the monotonically decreasing $\hat{P}(X)$ causes all obtained configurations to have the field lines closed in the equatorial plane and there is no X line anywhere in the magnetotail.

[41] Now focusing on the realistic configuration with $m = 0.35$, in Figure 5 we plot the plasma and total pressures as a function of α and distance, while Figure 6 shows the perpendicular current density j_Y in the midnight meridian plane. The current in the interior region is very similar to that obtained before in 3-D computations [*Zaharia and Cheng*, 2003a]. The tail current is concentrated in the plasma sheet, which has a width almost constant in Z (half width of 4 R_E) from 20 down to 75 R_E. As also obtained in 3-D computations, the ring current and the cross-tail current are not distinct current systems, with the transition between them rather gradual.

4.2. Prescribing $P(\alpha)$ and the Outer Flux Surface

[42] In this case we use as input the plasma pressure $P(\alpha)$ and the shape of the outer flux surface $a(X)$, while the solution gives the total pressure $\hat{P}(X)$. This is a boundary value problem, similar to that treated before in the tail by *Birn* [1991]. We again take in the inner closed region a spatially given pressure profile, with an analytical continuation in the "open" region given by (18).

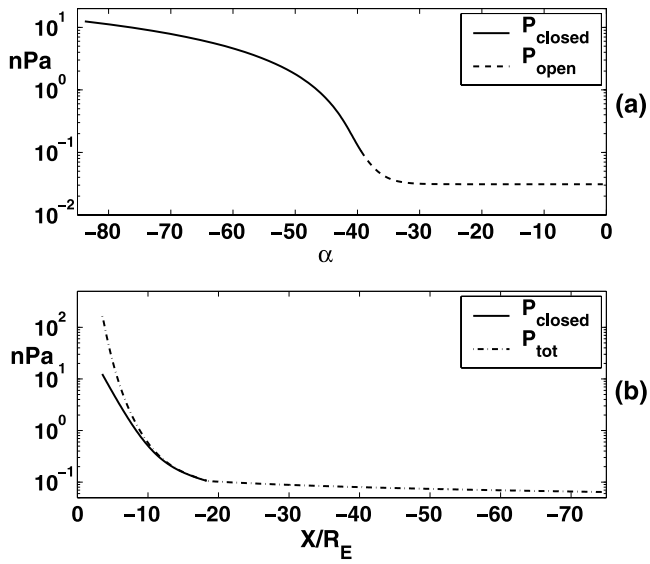

Figure 5. Quiet-time equilibrium with plasma pressure and $\hat{P}(X)$ ($m = 0.35$) inputs. (a) Pressure (in nPa) as a function of the flux function α. The solid (dashed) line shows pressure in the closed (open) field region. (b) Pressure in the closed field region (solid line) and total pressure on the equatorial plane at midnight (dash-dotted line).

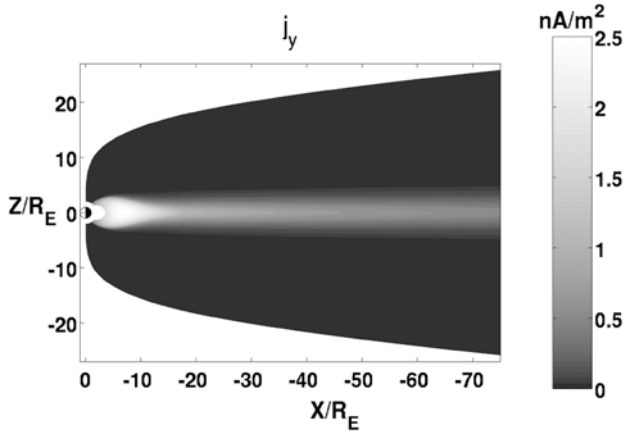

Figure 6. Current density j_Y for the quiet-time equilibrium with plasma pressure and $\hat{P}(X)$ ($m = 0.35$) inputs.

[43] For the shape of the flux boundary, we use field line mapping with the T96 empirical model [*Tsyganenko and Stern*, 1996]. The equation for the boundary location as a function of $\hat{P}$ can be straightforwardly obtained from equations (20) and (18) by imposing $\alpha = 0$:

$$a(\hat{P}) = \frac{\sqrt{2}(\alpha_n - \alpha_1)}{C|X_0|\sqrt{\hat{P} - P_0}} \operatorname{arctanh} \sqrt{1 - \frac{P_N - P_0}{\hat{P} - P_0} \exp\left\{\frac{C\alpha_n}{\alpha_n - \alpha_1}\right\}}. \tag{21}$$

[44] We however know now $a(X)$, therefore we can find $\hat{P}(X)$ numerically by inverting the expression above for $a(\hat{P})$ at each X. Because of the chosen monotonicity in $P(\alpha)$, $a(\hat{P})$ is monotonic, however $a(X)$ or $\hat{P}(X)$ need not be. Once $\hat{P}(X)$ is known, the tail equilibrium solution, equation (14), can be integrated and gives the magnetic field lines in the tail region through equation (20).

[45] Below we present results for the boundary value problem in two cases, a quiet- and a disturbed-time configuration. To allow comparison with results previously obtained for interior 3-D equilibria [*Zaharia and Cheng*, 2003a; *Zaharia et al.*, 2004] we use the same pressure profiles in the inner closed field region, as well as the same parameters in the T96 model.

4.2.1. Quiet-Time Equilibrium

[46] For obtaining the outer boundary in this case we use the T96 model with the quiet-time parameters described before. In the inner region we again consider the Spence-Kivelson pressure, equation (17), and we extend it in the "open field" region through equation (18). For the plasma pressure in the lobes we take $P_0 = 0.03$ nPa, which is on the order of magnitude typical of quiet times as discussed before.

[47] The equilibrium is achieved after 25 iterations. In the final state, Figure 7a shows the plasma pressure as a function of α. The decrease with α becomes very steep from a certain α value on, such that in the lobes the pressure is practically constant. Figure 7 also shows the variation of the pressure with distance in the "closed field" region, as well as that of $\hat{P}$ everywhere. One can see in Figure 7c a weak minimum in $\hat{P}$ at around $-60\ R_E$, which has implications for the **B** field configuration as we will see.

[48] In Figure 8 we plot several magnetic field lines of the obtained equilibrium. Of interest is the existence of an X line at around $-60\ R_E$ in the tail, where $\hat{P}$ is minimum (and also corresponding to the maximum in the tail radius). This is an effect due to the shape of the outer boundary from T96, which has a weak maximum there. This would present topology problems if an equilibrium solution were to be attempted numerically using the interior model (for which nested flux surfaces are needed). However, such a solution with an X line can be obtained in the form $Z(\alpha, X)$ using the tail model because we find $\hat{P}$ at each X location by inverting $a(\hat{P})$, but without requiring monotonicity in $\hat{P}(X)$ [*Birn*, 1991].

[49] Finally, we present in Figure 9 the perpendicular current density j_Y. It is quite similar to that obtained before, and also very similar in the inner region to what we obtained in previous 3-D computations [*Zaharia and Cheng*, 2003a; *Zaharia et al.*, 2004]. This is in spite of the ability of the last closed flux surface to vary in this computation, as opposed to previous calculations where it was kept fixed. The current is strongest close to Earth, forming the ring current. As before, the transition between this ring current and the "cross-tail" current is gradual. The cross-tail current extends all the way down the tail, with only slightly diminishing current density.

4.2.2. Disturbed-Time Equilibrium

[50] Here we present the solution of the boundary value problem for a disturbed time. We use similar inputs (but in

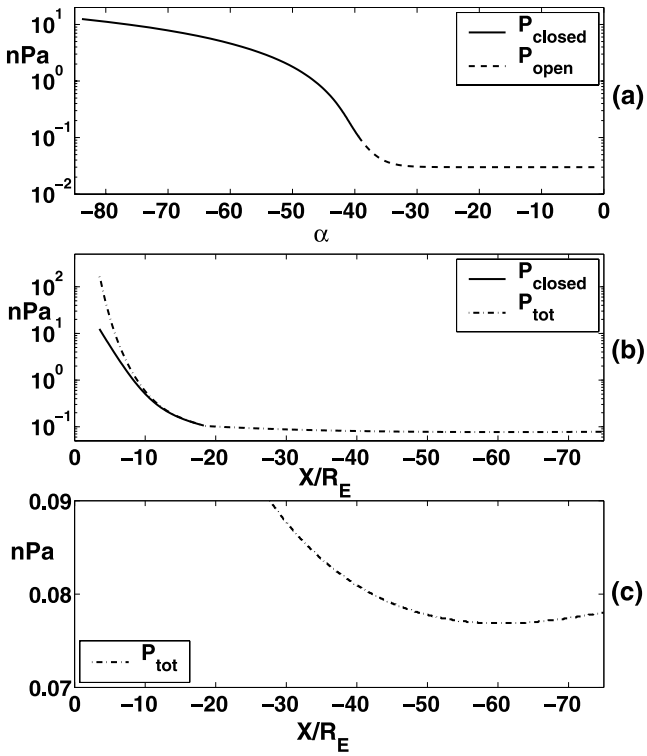

Figure 7. Quiet-time boundary value problem. (a) Pressure (in nPa) as a function of α. Solid (dashed) line shows pressure in the closed (open) field region. (b) Pressure in the closed region (solid line) and total pressure on the equatorial plane at midnight (dash-dotted line). (c) Enlargement of Figure 7b, showing a minimum in $\hat{P}$ at $\simeq -60\ R_E$.

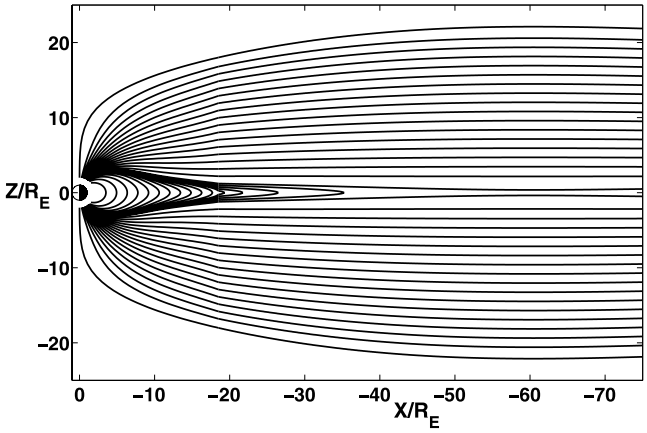

Figure 8. Magnetic field lines in the quiet-time boundary value equilibrium. An X line is located at $\simeq -60\ R_E$.

2-D) to those used before for the interior region in 3-D [*Zaharia and Cheng*, 2003a], as representing typical conditions during a substorm growth phase. Specifically, the outer magnetic flux surface is chosen using T96, with the disturbed-time parameters: $B_{\mathrm{ZIMF}} = -5$ nT, $B_{\mathrm{YIMF}} = 0$, $Dst = -50$ nT and $P_{\mathrm{SW}} = 5$ nPa.

[51] For the plasma pressure we also take the same form in the inner closed field region in the midnight meridian plane as in our previous study [*Zaharia and Cheng*, 2003a]:

$$P(X)|_{Z=0} = 12.5e^{-0.25|X|} \cdot \left[1.25 + 0.75\tanh\left(\frac{X_1 - |X|}{\Delta X}\right)\right] + 8.9|X|^{-1.53}, \quad (22)$$

with $X_1 = 10$ and $\Delta X = 1.25$. Equation (22) takes into account the increase seen in the plasma pressure values during the substorm growth phase (the increase is everywhere, but is higher at smaller radial distances). We use the same analytical continuation in the open field region, equation (18); however, with the lobe pressure higher in this case, $P_{\mathrm{lobe}} = 0.225$ nPa (the pressure is higher in the compressed lobes because of the higher solar wind pressure). The constant C in equation (18) is again found

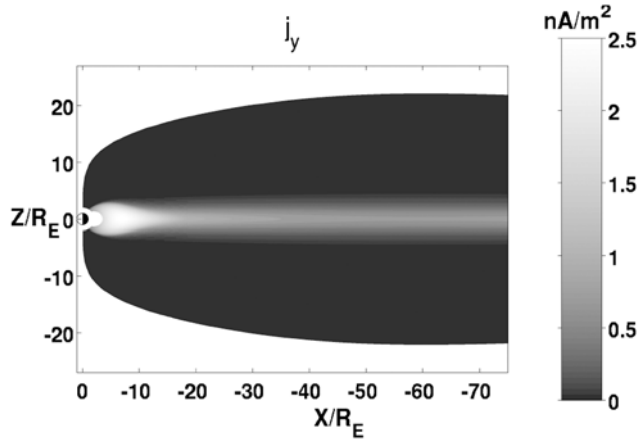

Figure 9. Electric current density j_Y for the quiet-time equilibrium with plasma pressure and $a(X)$ inputs.

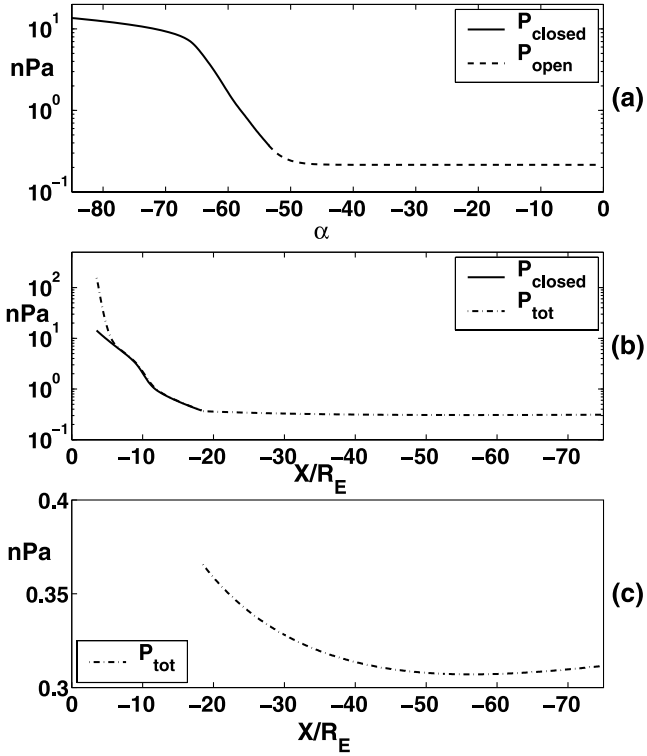

Figure 10. Disturbed-time boundary value problem. (a) Pressure (in nPa) as a function of the flux function α. Solid (dashed) line shows pressure in the closed (open) field region. (b) Pressure in the closed field region (solid line) and total pressure on the equatorial plane, midnight meridian (dash-dotted line). (c) Enlargement of Figure 10b, showing a local minimum in $\hat{P}$ at around $-55\ R_E$.

such that the pressure and its derivative are continuous at the open-closed boundary. For this computation, C is found to be smaller than in the quiet-time case, showing a less abrupt decrease of P with increasing α.

[52] For this case we show the plasma pressure as a function of α in Figure 10a. Figure 10 also presents $\hat{P}(X)$, with a minimum in $\hat{P}$ here as well, at around $\simeq -55\ R_E$.

[53] The field lines of the disturbed-state equilibrium are shown in Figure 11. An X line is visible at about $-55\ R_E$ in the tail. Finally, Figure 12 shows the perpendicular current density. We use a scale up to 2.5 nA/m^2 only in order to compare to the quiet-time case (the current in the inner region saturates at about 11 nA/m^2 as before [*Zaharia and Cheng*, 2003a].) The interior current is very similar in shape and magnitude to the one obtained before with the same pressure profile. The higher current extends in the tail, where the current density has lower values than near Earth, but higher than in the quiet-time case.

5. Discussion

[54] The present work demonstrates the feasibility of applying a line-tying approach to couple the two equilibrium models. A notable advantage of this technique vs. purely numerical approaches is that the magnetotail part is given by asymptotic theory and only entails solving

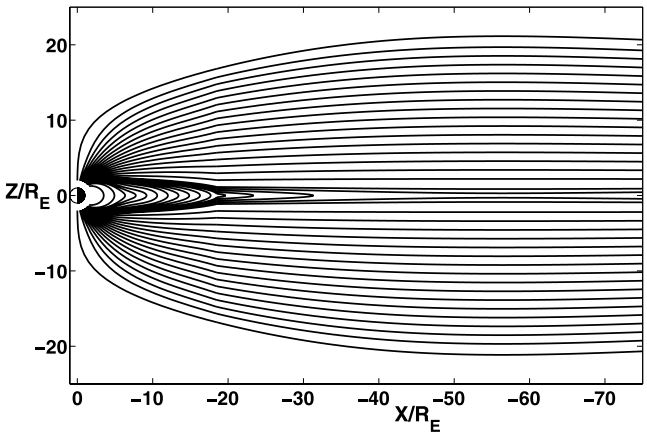

Figure 11. Several **B** field lines in the disturbed-time equilibrium. A far-tail neutral line is located at $\simeq -55\ R_E$.

ordinary differential equations and integrals. This is much faster than purely numerical equilibrium calculations (i.e., solving the Grad-Shafranov equation or the more complex 3-D equations in flux coordinates or via the magnetofrictional method). Since the tail solution is found by separate integration for each field line, it can be sought with arbitrary accuracy; at the same time, this allows the concentration of numerical resources (grid points) in the inner magnetosphere.

[55] Our results also show how coupled equilibrium solutions depend on different combinations of flux boundary conditions and plasma parameters taken as inputs. The input quantities have to be realistic; however, with some inputs, the approach does not guarantee the existence of a solution. For example, in the boundary value problem, given the shape of the outer flux surface, it is clear from equation (21) that in order for a solution to exist P_0 (close to $P_{\rm lobe}$) cannot be too large.

[56] Two restrictions of the present technique need to be mentioned. While this paper is more of a proof of principle for the line-tying approach, the coupled model can be straightforwardly employed in several applications, such as particle tracing or mapping of satellite data. For some purposes however further smoothing might be necessary near the coupling boundary; this is because while the inner model gives an exact (to the numerical accuracy) solution, the tail model is an asymptotic approximation; line tying at one plane, while guaranteeing continuity in the Euler potentials, might not guarantee it in their derivatives (i.e., the field itself) right at the boundary (leading to an ''infinitely thin'' current sheet, of finite but small current, there). A solution would be a finite-width buffer zone that would be set up to match the field and its derivative at its left and right boundaries and to interpolate between them inside.

[57] The other limitation has to do with the way of solving the equilibrium problem in the interior region. Specifically, the total magnetic flux is fixed inside the near-Earth ''closed field'' region, so realistic choices for the magnetic flux boundary conditions are very important. While we have no reason to question the ability of the T96 model of providing a good estimate of the outer flux boundary, the future solution to this limitation would be to solve a free -boundary equilibrium instead of the current fixed-boundary problem.

[58] Future work will also extend the computation to the three-dimensional case. To tackle the full 3-D problem, the line-tying approach presented here will be extended to the β equation as well. Since the computation of 3-D equilibria is an iterative sequence of solving quasi 2-D Grad-Shafranov-like equations, such an approach will permit the coupling in three dimensions. However, while the first coupling approach presented (specifying P and $\hat{P}(X)$) is directly extendable to 3-D, the boundary value case might not straightforward. A direct prescription of the magnetopause boundary or some equivalent flux surface is possible for the inner 3-D model, however only possible in the tail model for 2-D solutions [*Birn*, 1991] and a limited class of 3-D solutions [*Birn*, 2005], but not for the general case yet.

6. Summary and Conclusions

[59] In this paper we present first results (specifically, the two-dimensional case) from coupling two approaches of obtaining magnetospheric equilibria: a numerical flux coordinate method that solves the equilibrium in the inner/middle magnetosphere, and an asymptotic ''tail approximation'' farther away from Earth. The two approaches work best in complementary regions and both express the magnetic field in terms of Euler potentials, allowing their coupling through a ''line-tying'' technique.

[60] The problem is solved by specifying two out of three possible inputs: plasma pressure P, total pressure variation in the tail $\hat{P}(X)$, and the shape of the outer magnetic flux surface (close to the magnetopause), $a(X)$. We present solutions for both a quiet time and a substorm growth phase. Our focus is the boundary value problem, whereby we specify the shape of the outer flux surface and the pressure, while $\hat{P}(X)$ is an output of the model. The results in the interior region for both the quiet and the disturbed time resemble midnight meridian profiles obtained before in 3-D [*Zaharia and Cheng*, 2003a; *Zaharia et al.*, 2004]. The solutions for the tail region are found in analytical form for the particular pressure functions used. They can be easily found by numerical integration in the more general case however.

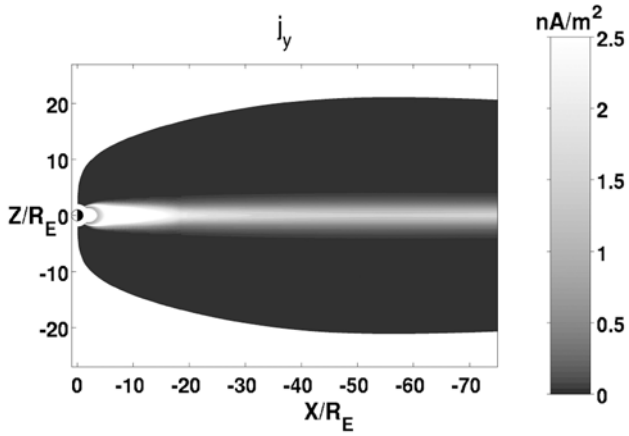

Figure 12. Electric current density j_Y for the disturbed-time equilibrium with plasma pressure and $a(X)$ inputs.

[61] Besides showing the feasibility of using a line-tying approach to solve a magnetospheric equilibrium problem, the current work treating the 2-D case is relevant to the future 3-D model coupling, as the 3-D numerical solution consists of an iterative sequence of 2-D solutions. Future work will thus include the extension of the line-tying approach to the full 3-D case, by also applying the line-tying to the other Euler potential (β) in the equilibrium equations. While noting that the states described here were computed independently by specifying distinct input parameters and thus are not connected in any way, in the future we will also describe the magnetospheric evolution as a sequence of computed quasi-static equilibria, linked together through conservation laws such as topology and entropy conservation.

[62] **Acknowledgments.** This work was performed under the auspices of the U.S. Department of Energy, with LANL support for S. Zaharia in the form of an LDRD director's fellowship. Additional support is acknowledged from the U.S. Department of Energy's Office of Basic Energy Sciences through its Geosciences Research Program, NASA's Sun-Earth Connection Theory Program, and the National Science Foundation through grant ATM-0202306.

[63] Lou-Chuang Lee thanks Heinz Wiechen and the other reviewer for their assistance in evaluating this paper.

References

Birn, J. (1987), Magnetotail equilibrium theory: The general three-dimensional solution, *J. Geophys. Res.*, *92*, 11,101.

Birn, J. (1991), The boundary value problem of magnetotail equilibrium, *J. Geophys. Res.*, *96*, 19,441.

Birn, J. (2005), Three-dimensional magnetospheric equilibria with prescribed boundary shapes, *J. Geophys. Res.*, *110*, A07203, doi:10.1029/2004JA010869.

Birn, J., G. Yur, H. U. Rahman, and S. Minami (1992), On the termination of the closed field line region of the magnetotail, *J. Geophys. Res.*, *97*, 14,833.

Birn, J., J. C. Dorelli, M. Hesse, and K. Schindler (2004), Thin current sheets and loss of equilibrium: Three-dimensional theory and simulations, *J. Geophys. Res.*, A02215, doi:10.1029/2003JA010275.

Cheng, C. Z. (1995), Three-dimensional magnetospheric equilibrium with isotropic pressure, *Geophys. Res. Lett.*, *22*, 2401.

De Michelis, P., I. A. Daglis, and G. Consolini (1999), An average image of proton plasma pressure and of current systems in the equatorial plane derived from AMPTE/CCE-CHEM measurements, *J. Geophys. Res.*, *104*, 28,615.

DeLucia, J., S. C. Jardin, and A. M. M. Todd (1980), An iterative metric method for solving the inverse tokamak equilibrium problem, *J. Comput. Phys.*, *37*, 183.

Fairfield, D. H., and J. Jones (1996), Variability of the tail lobe field strength, *J. Geophys. Res.*, *101*, 7785.

Harris, E. G. (1962), On a plasma sheath separating regions of oppositely directed magnetic field, *Nuovo Cimento*, *23*, 115.

Hesse, M., and J. Birn (1993), Three-dimensional magnetotail equilibria by numerical relaxation techniques, *J. Geophys. Res.*, *98*, 3973.

Lee, L. C., L. Zhang, G. S. Choe, and H. J. Cai (1995), Formation of a very thin current sheet in the near-Earth magnetotail and the explosive growth phase of substorms, *Geophys. Res. Lett.*, *22*, 1137.

Lemon, C., F. Toffoletto, M. Hesse, and J. Birn (2003), Computing magnetospheric force equilibria, *J. Geophys. Res.*, *108*(A6), 1237, doi:10.1029/2002JA009702.

Lui, A. T. Y., and D. C. Hamilton (1992), Radial profiles of quiet time magnetospheric parameters, *J. Geophys. Res.*, *97*, 19,325.

Mouschovias, T. C. (1974), Static equilibria of the interstellar gas in the presence of magnetic and gravitational fields: Large-scale condensations, *Ann. Phys.*, *192*, 37.

Press, W. H., S. A. Teukolsky, W. T. Vetterling, and B. P. Flannery (1992), *Numerical Recipes in FORTRAN 77: The Art of Scientific Computing*, 2nd ed., 859 pp., Cambridge Univ. Press, New York.

Shue, J.-H., J. K. Chao, H. C. Fu, C. T. Russell, P. Song, K. K. Khurana, and H. J. Singer (1997), A new functional form to study the solar wind control of the magnetopause size and shape, *J. Geophys. Res.*, *102*, 9497.

Siscoe, G. L. (1972), Consequences of an isotropic static plasma sheet in models of the geomagnetic tail, *Planet. Space Sci.*, *20*, 937.

Slavin, J. A., E. J. Smith, D. G. Sibeck, D. N. Baker, R. D. Zwickl, and S.-I. Akasofu (1985), An ISEE-3 study of average and substorm conditions in the distant magnetotail, *J. Geophys. Res.*, *90*, 10,875.

Spence, H. E., and M. G. Kivelson (1993), Contributions of the low-latitude boundary layer to the finite width magnetotail convection model, *J. Geophys. Res.*, *98*, 15,487.

Stern, D. (1970), Euler potentials, *Am. J. Phys.*, *38*, 494.

Takeda, T., and S. Tokuda (1991), Computation of MHD equilibrium of tokamak plasma, *J. Comput. Phys.*, *93*, 1.

Toffoletto, F. R., R. W. Spiro, R. A. Wolf, J. Birn, and M. Hesse (2001), Modeling inner magnetospheric electrodynamics, in *Space Weather*, edited by P. Song, H. J. Singer, and G. L. Siscoe, *Geophys. Monogr. Ser.*, vol. 125, p. 265, AGU, Washington, D. C.

Tsyganenko, N. A. (1987), Global quantitative models of the geomagnetic field in the cislunar magnetosphere for different disturbance levels, *Planet. Space Sci.*, *35*, 1347.

Tsyganenko, N. A. (2000), Solar wind control of the tail lobe magnetic field as deduced from Geotail, AMPTE/IRM, and ISEE 2 data, *J. Geophys. Res.*, *105*, 5517.

Tsyganenko, N. A. (2002), A model of the near magnetosphere with a dawn-dusk asymmetry: 2. Parameterization and fitting to observations, *J. Geophys. Res.*, *107*(A8), 1176, doi:10.1029/2001JA000220.

Tsyganenko, N. A., and D. P. Stern (1996), Modeling the global magnetic field of the large-scale Birkeland current systems, *J. Geophys. Res.*, *101*, 27,187.

Wang, C. C. L., and K. Tang (2005), Non-self-overlapping Hermite interpolation mapping: A practical solution for structured quadrilateral meshing, *Comput. Aided Design*, *37*, 271–283.

Wiechen, H., and K. Schindler (1988), Quasi-static theory of the Earth's magnetotail, including the far tail, *J. Geophys. Res.*, *93*, 5922.

Wolf, R. A. (1983), The quasi-static (slow-flow) region of the magnetosphere, in *Solar-Terrestrial Physics: Principles and Theoretical Foundations: Based on the Proceedings of the Theory Institute Held at Boston College, August 9–26, 1982*, edited by R. L. Carovillano and J. M. Forbes, p. 303, Springer, New York.

Zaharia, S. (2003), 3-D magnetospheric structures and energetic particle injections, Ph.D. thesis, Princeton Univ., Princeton, N. J.

Zaharia, S., and C. Z. Cheng (2003a), Near-Earth thin current sheets and Birkeland currents during substorm growth phase, *Geophys. Res. Lett.*, *30*(17), 1883, doi:10.1029/2003GL017456.

Zaharia, S., and C. Z. Cheng (2003b), Can an isotropic plasma pressure distribution be in force balance with the T96 model field?, *J. Geophys. Res.*, *108*(A11), 1412, doi:10.1029/2002JA009501.

Zaharia, S., C. Z. Cheng, and K. Maezawa (2004), 3-D force-balanced magnetospheric configurations, *Ann. Geophys.*, *22*, 251, doi:1432-0576/ag/2004-22-251.

Zaharia, S., V. K. Jordanova, M. F. Thomsen, J. Birn, M. H. Denton, and C. Z. Cheng (2005), Effect of storm-time plasma pressure on the magnetic field in the inner magnetosphere, *Geophys. Res. Lett.*, *32*, L03102, doi:10.1029/2004GL021491.

J. Birn and S. Zaharia, Space Science and Applications, Los Alamos National Laboratory, P.O. Box 1663, MS D466, Los Alamos, NM 87545, USA. (szaharia@lanl.gov)

C. Z. Cheng, Princeton Plasma Physics Laboratory, Princeton University, Princeton, NJ 08543, USA.